RZ 3610 (# 99620) 05/16/2005
Electrical Engineering 8 pages

Research Report

Two Sensor Based H-infinity Control for Probe Storage

Aggeliki Pantazi, Abu Sebastian, Haris Pozidis, and Evangelos Eleftheriou

IBM Research GmbH
Zurich Research Laboratory
8803 Rüschlikon
Switzerland

Two sensor based H_∞ control for probe storage

Aggeliki Pantazi, Abu Sebastian, Haris Pozidis, Evangelos Eleftheriou
IBM Zurich Research Laboratory
CH-8803 Rüschlikon, Switzerland

***Abstract*— The ultra-high storage density in probe storage devices makes positioning a significant challenge. The probes have to be positioned over the storage medium with nanoscale accuracy. A feedback-control scheme based on a high-precision global-positioning sensor can provide the required accuracy. However, drift and low frequency noise affects the performance over long periods of operation. A novel control architecture based on the H_∞ control framework is presented which addresses this problem by using media derived positional information along with the global positioning sensor. This controller has a multiple input single output (MISO) structure and uses the best measurement in different frequency regions. Experimental results on a probe-storage device prototype demonstrate the efficacy of this approach.**

I. INTRODUCTION

Probe-storage devices are considered as an alternative to conventional data storage. In [1] an implementation of a probe-storage device is described that is based on a thermomechanical principle for storing/retrieving information written on thin polymer films. Digital information is stored by making indentations on the thin polymer film using the tip of atomic force microscope (AFM) cantilevers which are a few nanometers in diameter. For increased data rate an array of probes is used, where each probe performs read/write/erase operations over an individual storage field with an area of 100 μm $\times$ 100 μm.

The shape of a typical indentation resembles an almost conical structure with a diameter of approx. 15 to 30 nm. This implies that the probes have to be positioned with very high accuracy over the storage medium. A miniaturized scanner with x/y motion capabilities of about 120 μm is employed to position the probes over the storage medium. A control architecture for the MEMS scanner is presented in [2]. The x/y positional information was provided by thermal position sensors. Using these sensors, closed loop positioning resolution of around 2 nm has been demonstrated [3].

Even though the thermal sensors have satisfactory noise performance in the high frequency region, they tend to have a significant low frequency component due to ambient temperature variations. Hence a feedback-control scheme relying on the thermal sensors alone is not suitable for long term operation of the device.

Due to the availability of multiple probes, a few probes and their respective storage fields could be dedicated for the generation of some form of media-derived positional error signal (PES) [1]. This media-derived PES accurately captures deviations from the track centerline for each data track. However, the media derived PES has a very limited range of approx. 50 nm. Hence even though the media derived PES does not suffer from drift, a feedback scheme relying on that alone may not be appropriate for the storage device due to its limited range.

This motivated the design of a control architecture that utilizes both the thermal-sensor signal and the media derived PES. The objective of the design method presented here is to create a control structure that utilizes the best measurement in different frequency regions. With the a priori knowledge that the thermal sensors are less reliable at low frequencies, the positional information from the media derived PES is primarily utilized for control at low frequencies. In the same vein, the thermal position sensor signal with high fidelity at high frequencies and unlimited range is preferred over the PES signal at high frequencies.

The H_∞ control framework was found to be appropriate to address such a "frequency division control". The controller has a multiple input single output structure and the performance requirements are translated to appropriate weighting functions. In this paper we describe the solution to this problem and present its experimental validation on a probe-based storage prototype system. Note that the problem formulation is more general and can be applied to any control problem that has two sensors that have different performance characteristics in different frequency regions.

II. SYSTEM DESCRIPTION

A. Microscanner model

Assuming that the horizontal (x-direction) motion and the vertical (y-direction) motion are decoupled, the mechanical behaviour of the scanner in the x-(y-) directions can be modelled fairly accurately by two independent linear differential equations. Specifically, a second order model captures well the dynamics of the microscanner [2]. Figure 1 shows the frequency response for the y-axis model where the resonance frequency is at 138.1Hz and the quality factor is approximately 13.

Such a model does not capture the cross-coupling between the axes. Figure 2 shows the cross-coupling on the y-axis due to x-motion for various offsets in the y-direction. As shown in this figure the cross-coupling is nonlinear and position dependent. For the control design, the cross-coupling is treated as a disturbance signal that has to be rejected by the control. However, for simulation purposes, a simplified model of the cross-coupling is used. This model is a quadratic fit of the cross-coupling as a function of the x-position, where the coefficients of the second order equation are changing depending on the y-position. As shown in Fig.

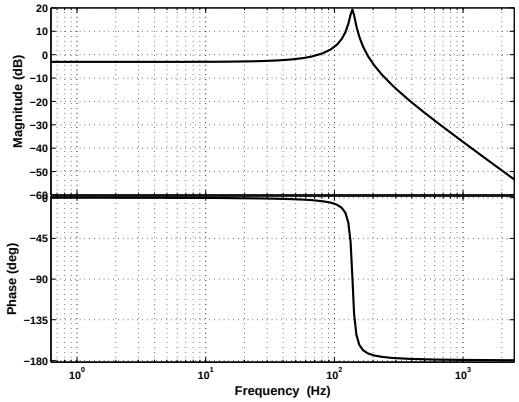

Fig. 1. Frequency response of the microscanner model in the y-axis

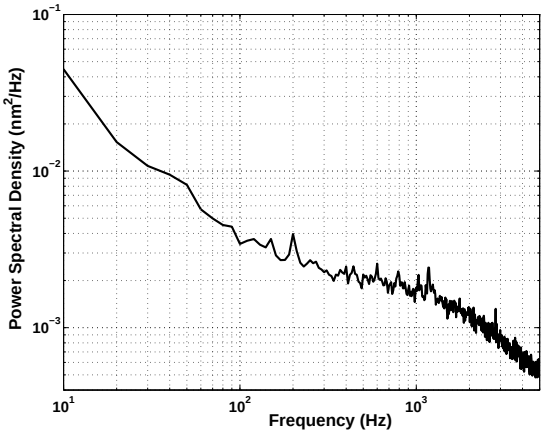

Fig. 3. Measured power spectral density of thermal-sensor noise

2 there is a very good match between the measured and the simulated cross-coupling.

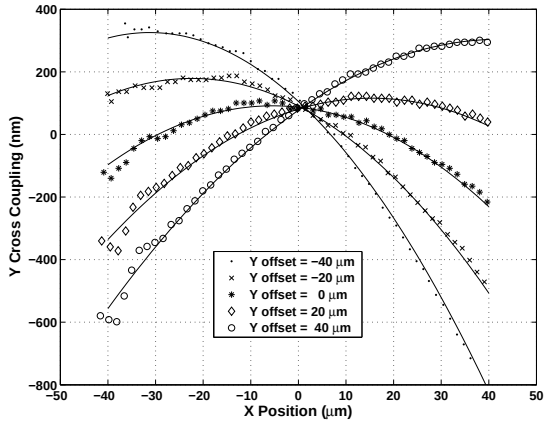

Fig. 2. Cross-coupling between the x- and y-axes. Marks represent the measured data and lines correspond to the quadratic fit.

B. Thermal position sensors

The thermal sensors do not introduce any additional dynamics, therefore can be modelled as constant gains. Positioning accuracy is related to the intrinsic noise characteristics of the sensors. The standard deviation of the sensor noise has been measured to be approx. 2 nm over 5 kHz bandwidth. Although the accuracy of the sensor is reasonably good there is a significant low frequency component as can be seen from the power spectral density of the sensor noise shown in Fig. 3.

The thermal sensors operate over the entire travel range of the micro-scanner and hence are capable of providing a global position information.

C. Media-derived position error signal (PES)

Besides the thermal position sensors, pre-written servo patterns on the medium can provide an alternate position signal. In fact, this signal measures the deviation from the track center while reading from that track. The method for generating this media derived PES is based on the concept of mutually vertically displaced sequences of indentations (bursts), arranged in such a way as to produce two signals in quadrature, which can be combined to provide a robust PES [1]. Servo bursts labeled A and B are used for the creation of the in-phase signal (I) and C and D for the quadrature signal (Q). A, B, C and D bursts are written in four different dedicated storage fields, called servo fields. The cross-track distance between the centers of the same burst is equal to the track pitch (TP), whereas the distance between the centers in A and B (or C and D) bursts is TP/2. The distance between A and C centers is TP/4. The configuration of the servo bursts is illustrated in Fig. 4. The circles represent the written indentations and the track centerlines coincide with the centers of burst B.

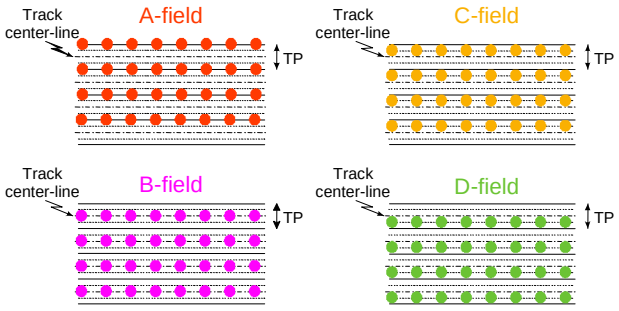

Fig. 4. Servo burst configuration

To illustrate the principle of PES generation let us assume that indentations in all bursts are spaced BP units apart in the x-direction, and that sampling occurs exactly at the indentation centers. Referring to Fig. 4, let us further assume that the cantilevers move in the y-direction following a line crossing the centers of the indentations. For example, the cantilever of the field A moves from the edge of the top indentation towards its center, then towards its bottom edge, then to a blank space, again to an indentation and so on. The amplitude of the readout signal is maximum at the indentation center and decreases with the distance from the

center. The I-signal is synthesized as the difference $\bar{A}-\bar{B}$, where $\bar{A}$ and $\bar{B}$ correspond to the measured signal amplitudes in bursts A and B, respectively. The Q-signal is generated from the readback signals of bursts C and D as $\bar{C}-\bar{D}$. Note that the Q-signal exhibits zero crossings at points where the I-signal has local extrema, as shown in Fig. 5. A certain combination of the two signals (I and Q), has zero crossings at all track center locations, and linear range between -TP/2 and TP/2.

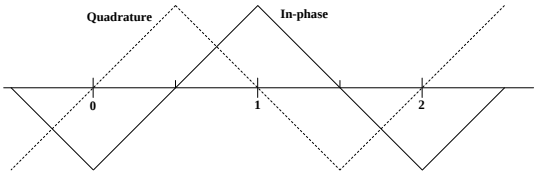

Fig. 5. Ideal position-error signal

The media derived PES provides positional information around each track centerline, therefore has a maximum range of TP. Moreover, a reliable PES is obtained only after the probes have traversed one BP while scanning in the x-direction. Hence, PES is a discrete signal with the discrete time step equal to the time taken by the scanner to move BP distance in the x-direction.

III. CONTROLLER DESIGN

A. Two-sensor-based control configuration

As mentioned earlier the objective is to design a joint controller that utilizes both the thermal sensor signal and the media derived PES. The block diagram describing such a control architecture is shown in Fig. 6. In this configuration, G denotes the nominal model of the plant, that is the microscanner model in the y-direction, and K represents the controller to be designed. We assume that we are operating around a track centerline so that media derived position information, y_{PES} is available. Positioning information from the thermal sensor is denoted by y_{th}.

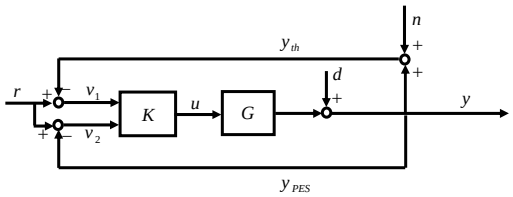

Fig. 6. Block diagram of two-sensor-based control configuration

The objective is to design this controller such that it is able to take advantage of the unlimited range and high fidelity of the thermal sensor signal at high frequencies and the low frequency accuracy of media derived PES. This problem can be formulated as a general control problem of a system that has two sensors with different noise characteristics at different frequencies. The objective is then to design a control structure that utilizes the best sensor at each frequency region.

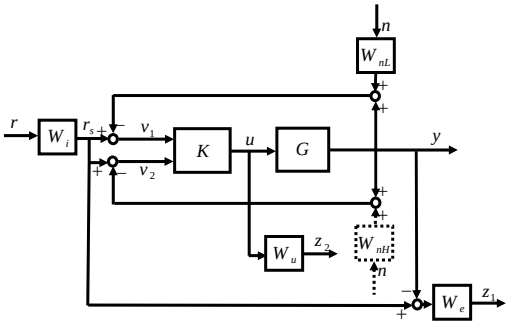

Fig. 7. Joint control formulation using weighting functions

A formulation of this problem is shown in the block diagram of Fig. 7. Weighting functions are used to characterize the frequency content of the input signals, i.e., the reference and the noise sources, but also to impose constraints on the tracking error and the control effort. Specifically, the weight W_i has a high gain at low frequencies and a roll-off rate of 20dB/decade in order to approximate as close as possible an integral term in the controller, which is required for zero steady-state error. The difference in noise characteristics of the two sensors is captured by the two weights W_{nL} and W_{nH}. The transfer function W_{nL} has low-pass filter characteristics that forces the signal v_1 to be the preferred signal at high frequencies. On the other hand, the transfer function W_{nH} exhibits high-pass filter characteristics that renders the signal v_2 to be the preferred one at low frequencies. For the system under consideration, the signal v_1 can model the thermal-sensor signal that has a significant low-frequency component. Finally, the media derived PES can be thought of as a second sensor with a fictitious high-frequency noise, since the requirement is to utilize more the thermal sensor signal at higher frequencies.

The weights W_e and W_u are used to impose constraints on the tracking error and the control signal, respectively. Since the constraint on the tracking error can be captured also by the weight W_i we set the weight W_e equal to 1.

This problem can be cast as an H_∞ optimization problem using the general control configuration shown in Fig. 8.

In this configuration, the exogenous input is $\mathbf{w}=\begin{bmatrix} r \\ n \end{bmatrix}$, where r denotes the reference and n represents the noise. Similarly, the error signal is $\mathbf{z}=\begin{bmatrix} z_1 \\ z_2 \end{bmatrix}$, where $z_1=W_e(r_s-y)$ and $z_2=W_u u$. The system can then be described by

$$\begin{bmatrix} \mathbf{z} \\ \mathbf{v} \end{bmatrix} = P \begin{bmatrix} \mathbf{w} \\ u \end{bmatrix} = \begin{bmatrix} P_{11} & P_{12} \\ P_{21} & P_{22} \end{bmatrix} \begin{bmatrix} \mathbf{w} \\ u \end{bmatrix}, \qquad (1)$$

$$u = K\mathbf{v},$$

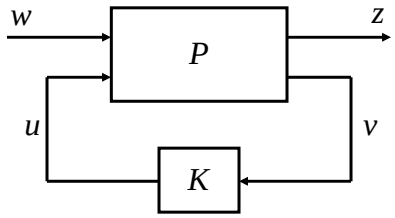

Fig. 8. General control configuration

where $\mathbf{v} = \begin{bmatrix} v_1 \\ v_2 \end{bmatrix}$ is the input to the controller and the elements of the generalized plant P are given by

$$P_{11} = \begin{bmatrix} W_e W_i & 0 \\ 0 & 0 \end{bmatrix}, P_{12} = \begin{bmatrix} -W_e G \\ W_u \end{bmatrix}, \quad (2)$$

$$P_{21} = \begin{bmatrix} W_i & -W_{nL} \\ W_i & -W_{nH} \end{bmatrix}, P_{22} = \begin{bmatrix} -G \\ -G \end{bmatrix},$$

and the controller to be designed has the structure $K = \begin{bmatrix} K_1 & K_2 \end{bmatrix}$. The linear fractional transformation $F_l(P,K)$, defined as $\mathbf{z} = F_l(P,K)\mathbf{w}$ is given by

$$F_l(P,K) = \begin{bmatrix} \frac{W_e W_i}{1+GK_1+GK_2} & \frac{W_e(GK_1W_{nL}+GK_2W_{nH})}{1+GK_1+GK_2} \\ \frac{W_u W_i(K_1+K_2)}{1+GK_1+GK_2} & \frac{-W_u(K_1W_{nL}+K_2W_{nH})}{1+GK_1+GK_2} \end{bmatrix}, \quad (3)$$

The objective of the standard H_∞ optimal control is to find a stabilizing controller K which minimizes, [4],

$$\left|\left|F_l(P,K)\right|\right|_\infty = \max_\omega \ \bar{\sigma}(F_l(P,K)(j\omega)). \quad (4)$$

In practice, we solve the H_∞ sub-optimal control problem where we find a stabilizing controller that gives an upper bound γ to the H_∞ norm [4]. That is,

$$\left|\left|F_l(P,K)\right|\right|_\infty < \gamma. \quad (5)$$

Note that the performance objectives are met if $\gamma \leq 1$.

Let S_{ref}, T_{noise}, and S_u be the closed-loop transfer functions from the reference r to the error $r-y$, from the noise n to the output y, and from the reference r to the control effort u, respectively. The equations that describe these transfer functions for the system shown in Fig. 6 are given by

$$S_{ref} = \frac{1}{1+GK_1+GK_2}, \quad (6)$$

$$T_{noise} = \frac{-GK_1}{1+GK_1+GK_2}, \quad (7)$$

$$S_u = \frac{K_1+K_2}{1+GK_1+GK_2}.$$

From (3) and (5) it is clear that the selection of the weight W_i gives an upper bound on S_{ref} and therefore captures the closed-loop tracking requirements. Also, the selection of the weights W_{nL} and W_{nH} determines the distribution of the gain of K_1 and K_2 as a function of frequency. This will eventually give the desired frequency response for T_{noise}. Finally, the weight W_u can be selected to provide an upper bound on the transfer function S_u, which limits the required control effort.

Equation (8), gives the expressions for T_{ref}, the transfer function from the reference to the output and S_{dis} the transfer function from the disturbances to the output. Specifically,

$$T_{ref} = \frac{GK_1+GK_2}{1+GK_1+GK_2}, \quad (8)$$

$$S_{dis} = \frac{1}{1+GK_1+GK_2}.$$

From these equations, we observe that the S_{dis} transfer function is equal to S_{ref} as in a one-degree-of-freedom control architecture. Therefore, the constraints imposed on S_{ref} are also valid for S_{dis}. Since our main disturbance is the cross-coupling that has similar frequency content as the reference signal there is no need for any additional constraints.

B. Joint controller design based on thermal sensor and media derived PES

A joint controller based on the thermal sensor signal and media derived PES was designed using the scheme described above. The microscanner and thermal-position sensor implementation characteristics along with the performance requirements were translated to appropriate weighting functions. The weighting function W_i was chosen as,

$$W_i = \frac{s+1257}{s+12.57}. \quad (9)$$

This selection was made to achieve a closed loop bandwidth of 200 Hz and to induce a 20 dB/decade slope for S_{ref} which approximates an integrator, required for zero steady state error tracking. The frequency region where the thermal-sensor information is not reliable can be specified by the weighting function W_{nL}, which was chosen as

$$W_{nL} = \frac{0.0001s+12.57}{s+0.1257}. \quad (10)$$

Since the thermal-sensor signal has a low-frequency component, W_{nL} is designed to have high gains at very low frequencies up to 2 Hz and low gains at high frequencies. The weighting function W_{nH} is given by (11) and it was chosen such that the joint controller relies more on the thermal sensor than the PES for frequencies higher than 50 Hz, that is

$$W_{nH} = \frac{s+0.03142}{s+314.2}. \quad (11)$$

Figure 9 depicts $\left|1/W_i\right|$, $\left|W_{nL}\right|$ and $\left|W_{nH}\right|$. The weighting function for the control, W_u was chosen to impose a constraint on the control effort.

A 5^{th} order controller with two inputs and one output is obtained from the design based on the H_∞ optimal control. The joint controller has a transfer function K_1 from the thermal sensor error signal to the output and a transfer function K_2 from the PES to the output as given in (12) and (13), respectively. Specifically,

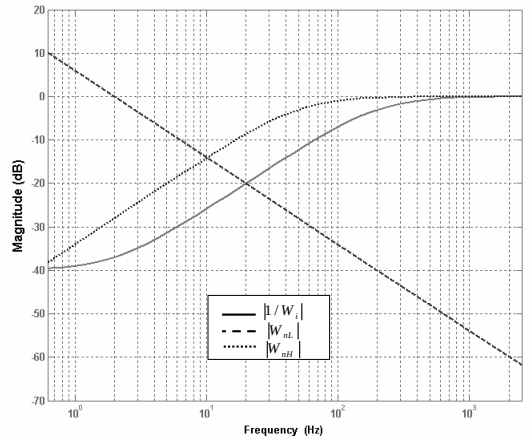

Fig. 9. Weighting transfer functions

$$K_1 = \frac{109600s(s^2+110.7s+13.9)(s^2+66.24s+7.529\times10^5)}{(s^2+69.55s)(s^2+57.8s+50.33)(s^2+10900s+5.897\times10^7)}, \quad (12)$$

$$K_2 = \frac{2119s(s^2+984s+2.104\times10^5)(s^2+66.24s+7.529\times10^5)}{(s^2+69.55s)(s^2+57.8s+50.33)(s^2+10900s+5.897\times10^7)}. \quad (13)$$

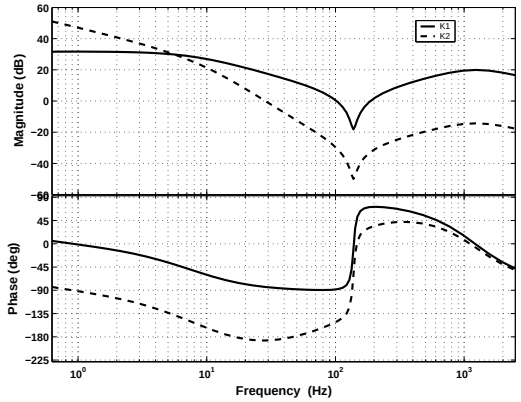

Fig. 10. Frequency response of the joint controller elements

Figure 10 shows the frequency response of the two elements K_1 and K_2 of the joint controller. The transfer function K_1 that uses as input the thermal-sensor signal has smaller gain at low frequencies than K_2 that uses as input the PES signal. At higher frequencies the transfer function K_1 has higher gain than K_2. The shape of the resulting transfer functions is in agreement with the design specifications. The point where the two transfer functions intercept, that specifies where each of the two inputs to the controller is more dominant, can be changed by modifying the appropriate weights W_{nL} and W_{nH}.

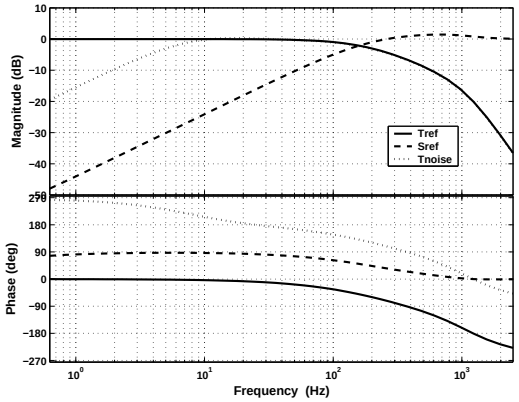

Fig. 11. Frequency response of closed loop transfer functions

Figure 11 shows the frequency response of the closed loop transfer functions T_{ref}, S_{ref}, and T_{noise}. The bandwidth of the closed loop system, that is the frequency where the magnitude of S_{ref} first crosses -3dB from below, is 130 Hz. Since S_{dis} is equal to S_{ref} the closed loop system can sufficiently reject disturbances approximately up to 130 Hz. The low gain of the T_{noise} at low frequencies is another good indication that the design meets the specifications since any noise input at these frequencies is not affecting the scanner motion.

IV. EXPERIMENTAL RESULTS

The proposed control architecture was implemented and demonstrated in an experimental set-up that includes the microscanner and the cantilever array chip. The performance of the joint control architecture is compared with that of the thermal sensor based control described in [3].

A. Media derived PES generation

For the purpose of generating media derived PES information, A, B, C and D bursts were written on the polymer medium using four cantilevers on their respective storage fields. The track pitch and bit pitch were set to 60 nm. Accordingly, the cross-track distance between the A(C) and B(D) bursts is equal to 30 nm. In order to depict the servo pattern a scan of 30 lines was performed stepping by 5 nm in the y-direction. Four samples of the readback signal per written indentation were used to correlate with a typical indentation shape and measure the indentation depth. The average indentation depth obtained over each line from the A, B, C and D servo fields is shown in Fig. 12.

The resulting in-phase and quadrature signals are shown in Fig. 13. We observe that the zero crossings of the quadrature signal align with the positions of the maximum signal of either A or B bursts with the zero crossing with positive slope corresponding to B bursts. In the implementation of the joint control architecture, only the quadrature signal is used as input to the controller with the track center line coinciding with the B bursts. Note that there is no loss of generality in

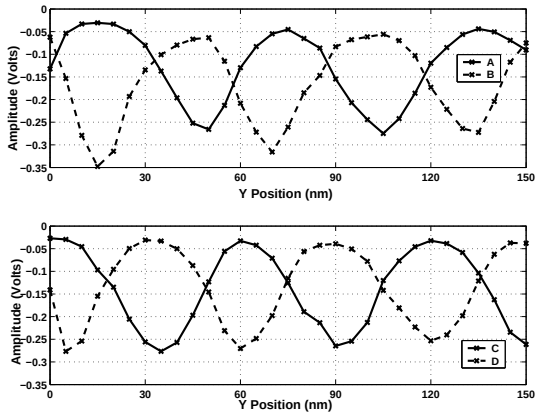

Fig. 12. A, B, C and D indentation profiles.

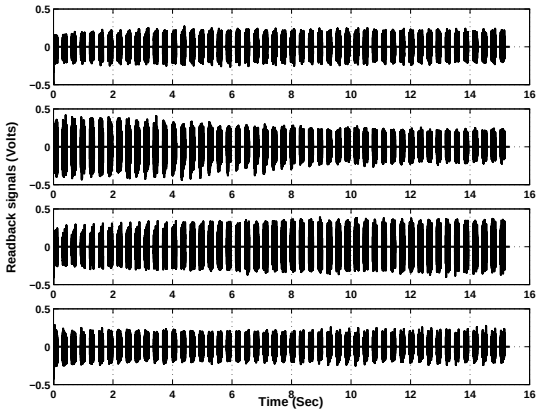

Fig. 14. Thermal sensors based control: Readback signal from the four cantilevers

the use of the quadrature signal alone. It solely results in a further reduction in the range of the position error signal.

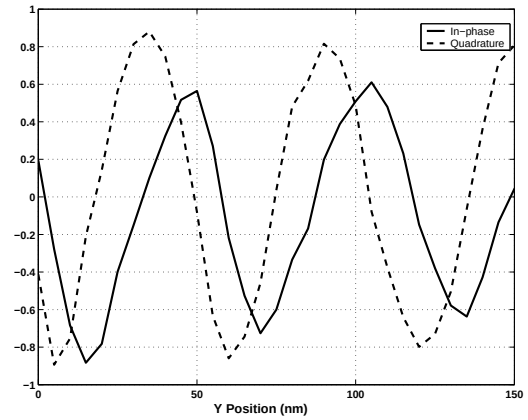

Fig. 13. In-phase and quadrature signals

B. Thermal-sensor based control

A servomechanism for the microscanner that uses the position information from the thermal sensors only, was presented in [2]. Specifically, two decoupled feedback loops for the x- and y-directions were designed based on the linear quadratic Gaussian approach with state estimation. Using this control scheme, we performed a simultaneous read operation using the four servo levers while scanning along the x-direction with a linear velocity of 0.3nm/μs. The reference signal on the y-axis is kept constant to a position close to the track centerline of servo lever B. Figure 14 shows the readback signal from the four servo fields for 50 scans.

We observe that although the y-axis reference is kept constant, the magnitude of the readback signal from servo field B is higher in the first few scans but decreases in the later scans. This means that the tip moves from a position close to the center of the indentations towards the edges and finally completely out of the indentations. On the contrary, the magnitude of the signal from servo field C is small in the first few scans but increases and stabilizes to a high value in the last scans. This can be better observed from the plot of the average magnitude of the indentation depth over each line scan that is shown in Fig. 15. This behavior can be explained by a possible drift on the thermal sensor signal that would be erroneously used by the controller to correct the position of the scanner. Since the distance between centers of bursts B and bursts C is equal to TP/4, in our case 15 nm, an estimated value of the drift is between 15 and 30 nm.

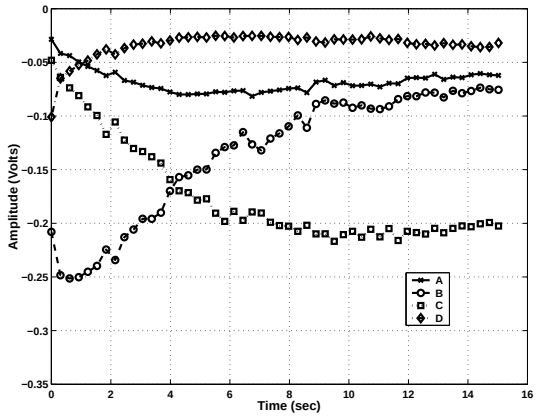

Fig. 15. Thermal sensors based control: A, B, C and D indentation profiles.

Another way to measure the motion in the y-direction is to use the control effort supplied by the controller. Subtracting the control effort of the first scan from that of the subsequent scans is a measure of the drift. This assumes that the cross coupling remains constant between successive scans which is valid since the motion in the x-axis remains the same for all scans and the y-reference is kept constant. Figure 16 shows the y-motion calculated from the control effort which shows that the estimated drift is 30 nm at the end of 50 scans, in accordance with the previous result. In the same figure, the y-motion as measured from the thermal sensors appears constant, as the control loop has corrected for the drift. This experiment clearly shows the adverse effect of the low frequency noise of the thermal position sensor.

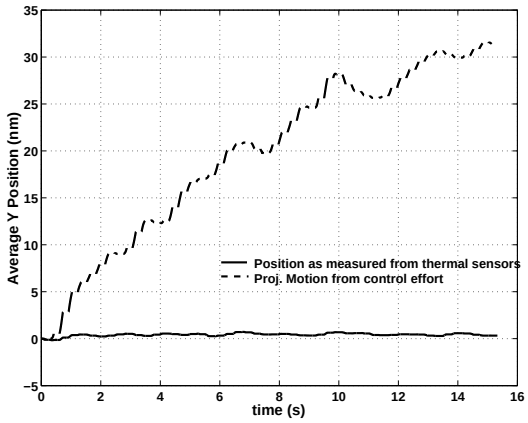

Fig. 16. Thermal sensors based control: y-sensor output and projected motion from the control effort

C. Joint control

The joint controller designed in the previous section has been realized in a digital signal processor. PES information is not available during seek and in negative scan directions since no read operation is performed. Therefore, both the thermal sensor and PES are active during the positive direction of the scan, and in the negative direction when no PES information is available, the PES signal is set to zero and control is given exclusively to the thermal sensors. As the controller is of the MISO type, there is no need to switch between different controllers when one of the sensor signals is not available.

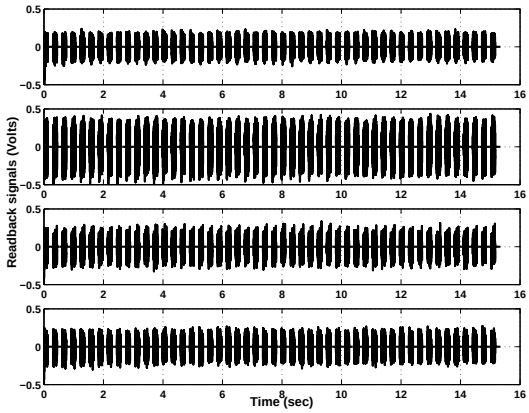

Fig. 17. Joint control: Readback signal from the four cantilevers

Using the joint control architecture we repeat the same experiment as described in the previous section. Figure 17 shows the readback signal from the four servo fields for 50 scans. Clearly, the magnitude of the signal from servo field B remains high throughout the experiment. Figure 18 shows the average magnitude of the indentation depth over each line scan. This result shows that the position of the probes is such that the cantilever of servo field B is always on top of the center of the indentation bursts B and the other three cantilevers are outside of the indentation bursts A,C and D. As the centers of indentation B were defined as the track centerlines, the tracking requirement is satisfied and tracking is immune to the low frequency noise from the thermal position sensors.

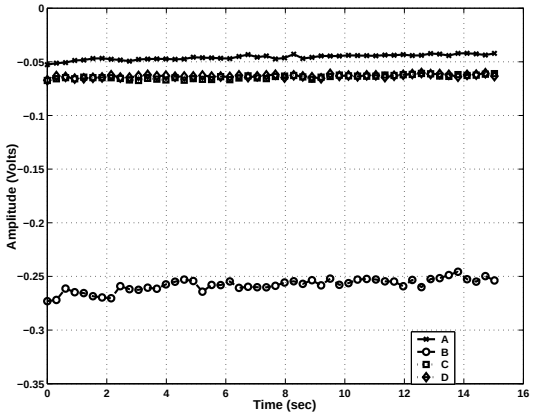

Fig. 18. Joint control: A, B, C and D indentation profiles.

The result can be verified again from the y-motion projected from the control effort as shown in Fig. 19. As can be seen, the y-motion remains constant although the signal from the thermal sensors indicates a motion of around 30 nm. Therefore, with this scheme the thermal sensor drift is not affecting the scanner motion.

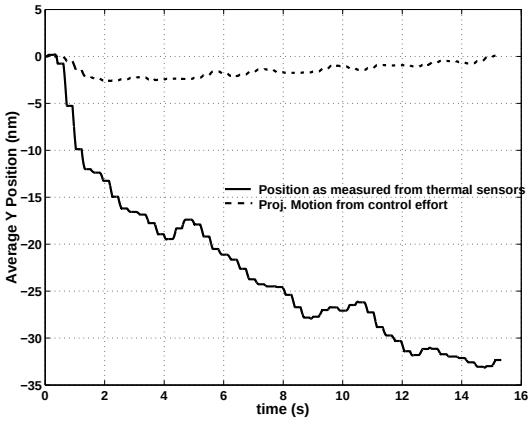

Fig. 19. Joint control: y-sensor output and projected motion from the control effort

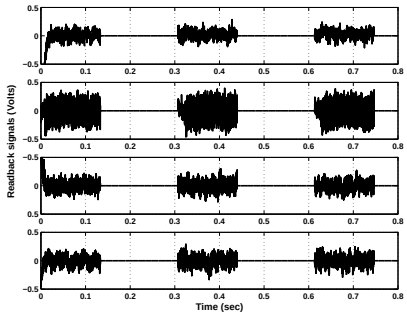

Fig. 20. Joint control: Readback signal from the four cantilevers

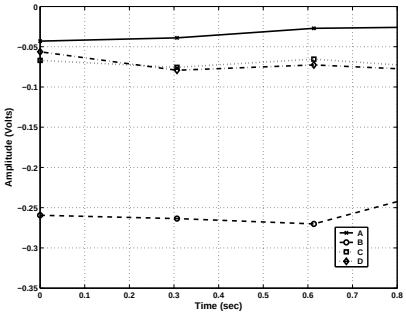

Fig. 21. Joint control: A, B, C and D indentation profiles.

Another experiment that verifies the robustness of the proposed joint controller architecture is that of navigation through the tracks. The readback signal from the four levers while navigating through three different tracks is shown in Fig. 20 and Fig. 21. Again we observe that the signal from cantilever B is highest throughout the experiment. This indicates that accurate probe positioning and subsequent track following, as required for reliable data storage, can be achieved using the proposed joint controller architecture.

V. ACKNOWLEDGMENTS

We thank our colleagues at the Storage Technologies and Nanomechanics groups at IBM Zurich Research Laboratory. Special thanks go to M. Lantz, M. Despont, U. Drechsler, D. Jubin and H. Rothuizen for the design and fabrication of MEMS parts, P. Bachtold for the design of the electronics used in this work and G. Cherubini for useful discussions.

REFERENCES

[1] E. Eleftheriou, T. Antonakopoulos, G. K. Binnig, G. Cherubini, M. Despont, A. Dholakia, U. Durig, M. A. Lantz, H. Pozidis, H. E. Rothuizen, and P. Vettiger. Millipede-a MEMS based scanning-probe data storage system. *IEEE transactions on magnetics*, 39(2):pp. 938–945, 2003.

[2] A. Pantazi, M. A. Lantz, G. Cherubini, H. Pozidis, and E. Eleftheriou. A servomechanism for a micro-electro-mechanical-system-based scanning-probe data storage device. *Nanotechnology*, 15:612–621, August 2004.

[3] A. Sebastian, A. Pantazi, G. Cherubini, E. Eleftheriou, M. Lantz, and H. Pozidis. Nanopositioning for probe storage. In *Proceedings of the American Control Conference, Portland, Oregon*, June 2005.

[4] S. Skogestad and I. Postlethwaite. *Multivariable Feedback Control, Analysis and Design*. John Wiley and Sons, 1997.